

USuRPER: Unit-Sphere Representation PERiodogram for full spectra

A. Binnenfeld¹, S. Shahaf², and S. Zucker¹

¹ Porter School of the Environment and Earth Sciences, Raymond and Beverly Sackler Faculty of Exact Sciences, Tel Aviv University, Tel Aviv, 6997801, Israel

e-mail: avrahambinn@gmail.com, shayz@tauex.tau.ac.il

² School of Physics and Astronomy, Raymond and Beverly Sackler Faculty of Exact Sciences, Tel Aviv University, Tel Aviv, 6997801, Israel

e-mail: sahar.shahaf@gmail.com

Accepted XXX. Received YYY

ABSTRACT

We introduce an extension of the periodogram concept to time-resolved spectroscopy. USuRPER – Unit Sphere Representation PERiodogram – is a novel technique which opens new horizons in the analysis of astronomical spectra. It can be used to detect a wide range of periodic variability of the spectrum shape. Essentially, the technique is based on representing spectra as unit vectors in a multidimensional hyperspace, hence its name. It is an extension of the phase-distance correlation (PDC) periodogram we had introduced in previous papers, to very high-dimensional data like spectra. USuRPER takes into account the overall shape of the spectrum, sparing the need to reduce it into a single quantity like radial velocity or temperature. Through simulations we demonstrate its performance in various types of spectroscopic variability — single-lined and double-lined spectroscopic binary stars and pulsating stars. We also show its performance on actual data of a rapidly oscillating Ap (roAp) star. USuRPER is a new tool to explore large time-resolved spectroscopic databases, e.g. APOGEE, LAMOST and the RVS spectra of *Gaia*. We have made available to the community a public GitHub repository with a Python implementation of USuRPER, to experiment with it and apply it to a wide range of spectroscopic time series.

Key words. methods: data analysis – methods: statistical – techniques: spectroscopic – binaries: spectroscopic – stars: oscillations – stars: individual: HD 115226

1. Introduction

In two previous papers (Zucker 2018, 2019), we have introduced the PDC (Phase Distance Correlation) periodogram as a new method to detect non-sinusoidal periodicities in unevenly-sampled time-series data. Essentially, for each trial period, PDC quantifies the statistical dependence between the measured quantity and the phase (according to the trial period), using the recently introduced *distance correlation*. Székely et al. (2007) had introduced distance correlation as a measure of statistical dependence between two quantities. The calculations involved in estimating the sample distance correlation somewhat resemble those involved in estimating the Pearson correlation, hence its name. However, it is important to note that unlike Pearson correlation, distance correlation is not a measure of linear dependence, but rather of general dependence.

In order to quantify the dependence on the phase, which is a circular variable (i.e. cyclic), we have modified the original expression of Székely et al. (2007), following their original derivation, but for circular variables. As we have shown (Zucker 2018), the newly introduced periodogram outperforms other methods in cases of sawtooth-like variability shapes, including also RV curves of eccentric single-lined spectroscopic binary (SB1) stars.

We have later extended the PDC periodogram to two-dimensional data (Zucker 2019), and specifically to two-dimensional astrometric data, so as to improve the detection of eccentric astrometric orbits. This generalization demonstrated an important advantage of distance correlation over the classic

Pearson correlation. Pearson correlation involves products of the sample values of the two examined variables, which means both of them have to be real numbers. Instead, distance correlation involves element-wise products of two matrices that are based on the distance matrices of the two variables. Thus, as long as distances can be calculated in each of the two examined spaces, there is no requirement regarding the dimensionality of the two variables. They can even be of different dimensions, as long as distance matrices can be computed.

Lyons (2013) further extended the applicability of distance correlation, by showing that it can be applied to variables in general metric spaces, as long as the two metrics involved are both of ‘strong negative type’. It is beyond the scope of this paper to get into the definition and subtleties of strong negative type metric spaces (first introduced in Zinger et al. 1992), but it is still important to note that Euclidean spaces are of strong negative type (Lyons 2013).

In this paper we introduce an extension of the PDC periodogram to a new domain: we propose to use it to detect general periodic variability of astronomical spectra. Perhaps the most obvious periodic variability of a stellar spectrum is that of SB1s, in which the spectra exhibit periodic Doppler shifts. The usual way to study SB1s is to cross-correlate the spectra against a template spectrum (either synthetic or observed), derive an estimate of the Doppler shifts from the location of the cross-correlation peaks (e.g. Tonry & Davis 1979) and then analyse the Doppler shifts in search for periodicity using conventional techniques,

like the GLS (Generalized Lomb-Scargle) periodogram (Ferraz-Mello 1981; Zechmeister & Kürster 2009).

Double-lined spectroscopic binaries (SB2s) exhibit a more complicated periodicity pattern, since each observed spectrum is essentially a superposition of two spectra, each shifted by a different Doppler shift, and both undergo opposite radial velocity changes. Occasionally, the cross-correlation of the spectrum against a template shows two peaks, but sometimes the two peaks blend, requiring the use of techniques to disentangle the two Doppler shifts, e.g. TODCOR (Zucker & Mazeh 1994).

Periodic variability of the spectrum need not necessarily be related to Doppler shifts in binary stars. Various types of stellar pulsations bring about many kinds of periodic variations of the spectrum, ranging from periodic temperature changes like in Cepheids (e.g. Andrievsky et al. 2005) to line-profile variations in non-radially pulsating stars (e.g. Aerts et al. 1992).

In the next Section we introduce the details of the calculations involved in producing the USuRPER periodogram. To demonstrate the capabilities of USuRPER, we show in Sect. 3 some test cases, both simulated and actually observed. We finally conclude in Sect. 4 with a short summary and some insights regarding applicability.

2. Unit-sphere representation periodogram

2.1. Fundamentals

Assume we have time-resolved spectroscopy data of an astronomical object, comprising N spectra obtained at times $\{t_i\}_{i=1}^N$. Let us further assume that each spectrum is essentially an array of L intensities, each corresponding to a specific wavelength. For simplicity, we assume at this stage that all spectra are calibrated to the same wavelength grid, and are all measured at the same rest frame. Those assumptions can later be easily relaxed by calibration and interpolation procedures that are routinely performed in astronomical spectroscopy and RV studies.

Since we are interested only in the variability of the spectrum shape (rather than the total flux), let us subtract the mean value of each spectrum and normalize it by dividing with its standard deviation. As a result, the spectra, $\{\hat{f}_i\}_{i=1}^N$, can be now considered unit vectors in an L -dimensional Euclidean space, i.e. points on the unit $(L-1)$ -sphere. Thus, should a periodic variability of the spectrum shape take place, it will be manifested in a periodic motion on this unit sphere.

We introduce here a novel kind of periodogram to look for this unit-sphere periodicity. Following our previous papers, we can construct such a periodogram by quantifying, for each trial period, the distance correlation between the location on the unit sphere and the phase (according to the trial period). For that, we need to have a distance function (metric) on the unit sphere, that will be of strong negative type. Such a metric can be defined by the length of the chord connecting two points on the sphere – the *chord-length metric*. This metric is of strong negative type since it is induced by the Euclidean metric of the L -dimensional space in which the unit sphere is embedded (Lyons 2013). As we now show, this metric is very easy to compute.

Let \hat{f}_i and \hat{f}_j be two members of the sequence of unit vectors introduced above. Let us denote by θ_{ij} the angle between those two unit vectors. By simple geometry we can immediately see that the chord length between the two corresponding unit-sphere locations is given by

$$d(\hat{f}_i, \hat{f}_j) = 2 \sin(\theta_{ij}/2) = 2 \sqrt{\frac{1 - \cos \theta_{ij}}{2}}. \quad (1)$$

Since \hat{f}_i and \hat{f}_j are unit vectors, $\cos \theta_{ij}$ is in fact the scalar product between them. In other words, it is actually the *normalized correlation between the two original spectra*, henceforth C_{ij} .

Now that we have defined a distance function, we could seemingly calculate the two required distance matrices, following Zucker (2018, 2019). However, the space on which our distance function (Eq. (1)) is defined is extremely high-dimensional, and as Székely & Rizzo (2013) show, a naive computation of the distance correlation in this case would introduce a very strong bias. They propose to use, instead, an *unbiased* estimate of the distance correlation, which we introduce in the next paragraphs.

2.2. Computation

Similarly to Zucker (2018, 2019), let us define a distance matrix based on the metric we have introduced in Eq. (1). For each pair of spectra (i and j), the entry in the distance matrix is:

$$a_{ij} = \sqrt{1 - C_{ij}}. \quad (2)$$

Note that we can safely remove the multiplicative factors appearing in Eq. (1), since they would later cancel out in the normalization.

For each trial period P let us define a phase distance matrix, similarly to the previous papers:

$$\begin{aligned} \phi_{ij} &= (t_i - t_j) \mod P, \\ b_{ij} &= \phi_{ij}(P - \phi_{ij}). \end{aligned} \quad (3)$$

Now, instead of the zero-centring used in the previous papers, which leads to a biased estimator of the distance correlation, we will apply \mathcal{U} -centring, introduced in Székely & Rizzo (2014) in order to mitigate the bias:

$$A_{ij} = \begin{cases} a_{ij} - \frac{1}{N-2} \sum_{k=1}^N a_{ik} - \frac{1}{N-2} \sum_{k=1}^N a_{kj} \\ \quad + \frac{1}{(N-1)(N-2)} \sum_{k,l=1}^N a_{kl} & \text{if } i \neq j, \\ 0 & \text{if } i = j. \end{cases} \quad (4)$$

A similar procedure is applied to obtain the matrix B_{ij} from b_{ij} . Using the \mathcal{U} -centred matrices the unbiased estimator of the distance correlation can be computed via the expression:

$$D = \frac{\sum_{ij} A_{ij} B_{ij}}{\sqrt{(\sum_{ij} A_{ij}^2)(\sum_{ij} B_{ij}^2)}}. \quad (5)$$

2.3. Run-time complexity

The matrix A_{ij} should be calculated only once. If the spectra are all calibrated to the same wavelength grid, each C_{ij} is a simple correlation coefficient, requiring $O(L)$ operations. However, since cross-correlation functions (CCFs) are routinely computed, especially in the context of RV studies, C_{ij} can also be extracted from the CCF, taking into account conversion to the rest-frame velocity. CCFs usually require $O(L \log L)$ operations (using fast convolution algorithms), which we henceforth use as a worst-case estimate. Therefore, calculating the matrix A_{ij} and

converting it to the \mathcal{U} -centred matrix a_{ij} involves $O(N^2 L \log L)$ operations. The matrix b_{ij} has to be calculated separately for each frequency, and then used in the calculation of the distance correlation (Eq. (5)), amounting to a total of $O(N^2 K)$, where K is the number of trial frequencies (periods). The total time complexity is therefore $\max[O(N^2 L \log L), O(N^2 K)]$ and it is a matter of specific implementation which of the two terms dominates. Whichever dominates, it is still a matter of quadratic dependence on the number of spectra. In future applications this quadratic dependence may be reduced to $O(N \log N)$ by using fast techniques to compute distance correlation that are now emerging (e.g. Huo & Székely 2016; Chaudhuri & Hu 2019).

3. Examples

3.1. Simulated SB1

In order to simulate spectra of an SB1, we used a synthetic solar-like spectrum ($T_{\text{eff}} = 5800$ K, $[\text{Fe}/\text{H}] = 0.0$, $\log g = 4.5$) from the spectral library PHOENIX (Husser et al. 2013), at a spectral resolution of $R = 10000$. We have simulated a simple sinusoidal RV curve (i.e. corresponding to a circular orbit), with a semi-amplitude of $K = 10 \text{ km s}^{-1}$ and a period of 7 days. We have randomly drawn 50 epochs from a uniform distribution on an interval of 100 days, and after shifting the spectrum according to the required RVs, we have added to the spectra white Gaussian noise, at an SNR of 100^1 . The wavelength range we have used for our simulations was $4900 - 5100 \text{ \AA}$.

The common approach to analyse such data is to cross-correlate each observed spectrum against an assumed template and estimate the location of the cross-correlation peak. Fig. 1 shows the resulting RV estimates thus obtained (using the PHOENIX spectrum as template). As is clearly evident from the Figure, the high SNR we had used in the simulation led to what seems to be a very smooth sinusoidal RV curve, with a negligible scatter around the sinusoid. This very well-defined periodicity, combined with the relatively large number of samples, is also manifested in a very sharp and prominent peak in the GLS periodogram at a frequency of $1/7 \text{ d}^{-1}$ (Fig. 2, lower panel). In fact, since the GLS is tailored to sinusoidal periodicities, we do not expect any other kind of periodogram to outperform the GLS in this case. Moreover, when we search for periodicity in the RV data, it means that we have already assumed that the spectroscopic variability is a Doppler-shift periodicity, and not, for example, line-profile variation.

Nevertheless, it is illuminating to compare GLS to our newly introduced periodogram. The upper panel of Fig. 2 shows the resulting USuRPER periodogram. Recalling that we have not extracted RVs in order to obtain this periodogram, it is very encouraging that USuRPER produced such a sharp peak at the correct period.

This example is a very simple case, with many samples and a high SNR, yet it serves as a kind of sanity check, and proves that this novel approach can indeed identify at least simple periodicities.

3.2. Simulated SB2

The case of SB2 is more challenging, since the spectroscopic variability is not merely a simple Doppler shift. We have sim-

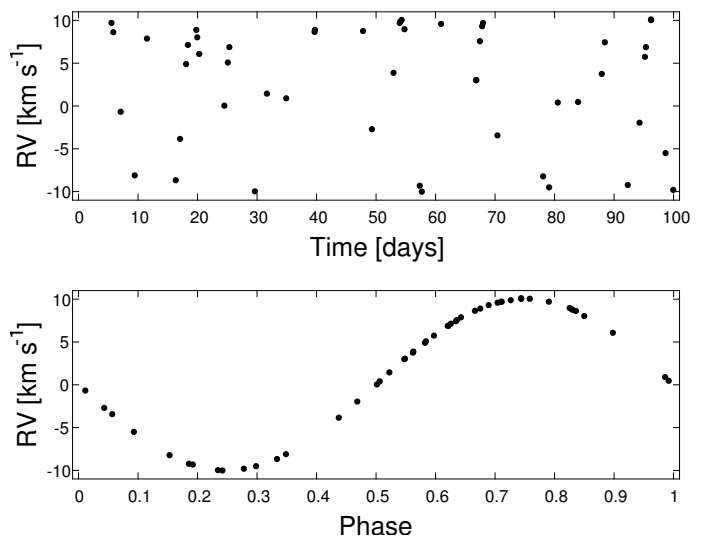


Fig. 1. Upper: estimated RV time series based on the simulated spectra of an SB1. Lower: the RV time series phase-folded by the known 7-day period.

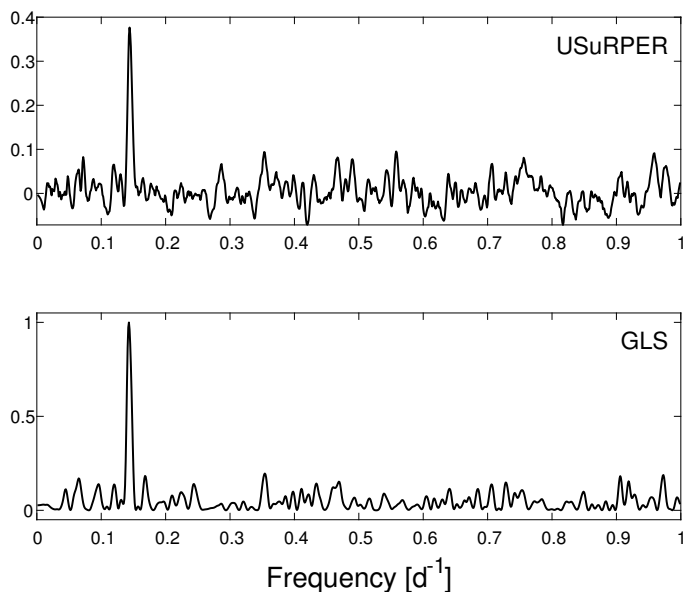


Fig. 2. GLS (lower panel) and USuRPER (upper panel) periodograms of the simulated SB1 whose RV are presented in Fig. 2. Note that both the GLS power and the distance correlation values of USuRPER are normalized and therefore unitless.

ulated SB2 data by using two PHOENIX spectra. We used the same solar-like spectrum we have used in the SB1 above as the spectrum of the primary component of the binary. For the secondary we used a spectrum corresponding to $T_{\text{eff}} = 5500$ K, $\log g = 4.5$ and $[\text{Fe}/\text{H}] = 0.0$. We shifted and blended the spectra, assuming a moderately eccentric ($e = 0.3$) 7-day Keplerian orbit. The orbital orientation was determined so that the maximal RV separation ($K_1 + K_2$) would be 10 km s^{-1} . In order to determine the individual semi-amplitudes K_1 and K_2 , as well as the intensity ratio for combining the spectra, we used the masses and radii listed in PHOENIX, assuming the two stars are main-sequence stars. In total, we sampled the simulated orbit at 20 epochs, with an SNR of 30. Fig. 3 presents the simulated primary and secondary RVs.

Fig. 4 demonstrates the challenge in this specific SB2 case. We show in the Figure two of the 20 spectra – at the largest and

¹ The SNR definition we used was the ratio between the continuum flux level and the noise standard deviation. We estimated the continuum flux level by the 98-th percentile of the flux values in the spectrum.

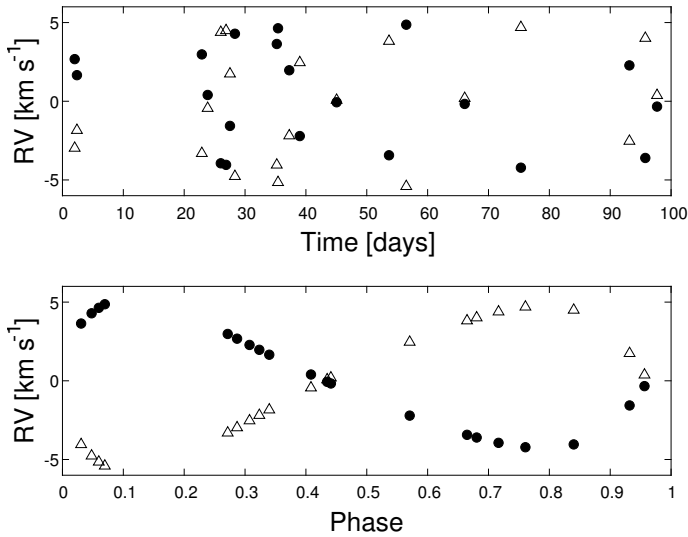


Fig. 3. Upper: the RV time series used in the SB2 simulation. Filled circles mark the primary RV and empty triangles the RV of the secondary. Lower: the same RV time series phase-folded by the known 7-day period.

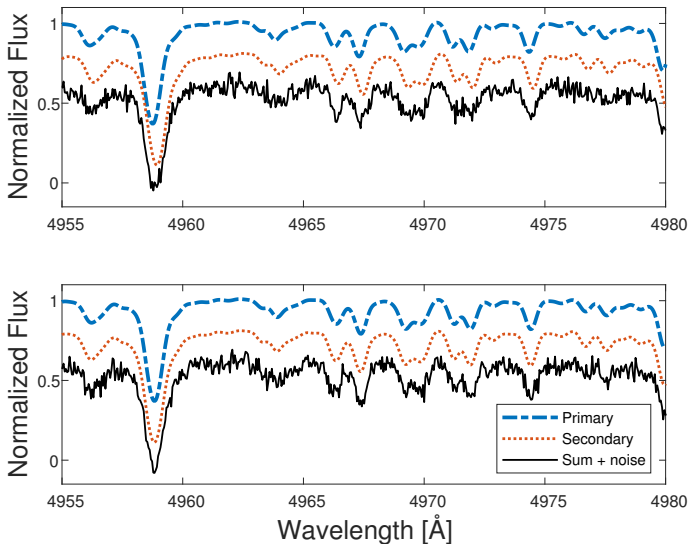


Fig. 4. A selected segment from two simulated SB2 spectra. The dashed blue lines represent the primary PHOENIX spectrum, while the red dotted lines represent the secondary. The black solid line is the combined and noised spectrum with an SNR of 30, used for the simulation. The spectra are normalized to a continuum level of 1. For clarity, a vertical offset of 0.2 was introduced to separate the spectra. The upper panel shows the spectrum with the maximum RV separation while the lower panel shows the one with the smallest separation.

smallest RV separation. The Figure focuses on the wavelength range 4955 – 4980 Å, which includes the Fraunhofer Iron c-line, at 4959.0 Å (note that we have not converted PHOENIX spectra from vacuum to air wavelengths). The Figure shows both components (with blue-dashed and red-dotted lines), and the composite noised spectrum (in black solid line). For clarity we have introduced vertical offsets among the three spectra in each panel. The challenge is obvious – at a resolution 10000 and SNR 30 it is practically impossible to disentangle the two components. The main effect of the varying RV separation seems to be a minute change in the width and depth of the composite spectral lines.

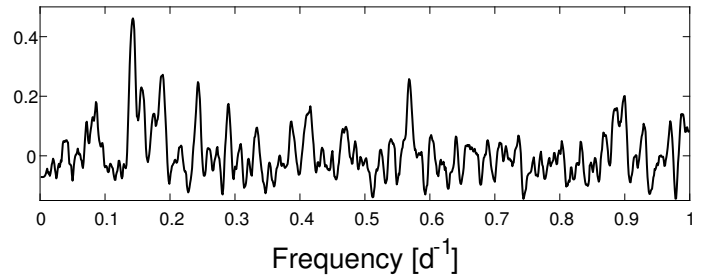


Fig. 5. USuRPER periodogram plot for the simulated SB2 case. Note that the distance correlation values of USuRPER are normalized and therefore unitless.

Fig. 5 presents the resulting USuRPER periodogram. In spite of the challenge posed by the low resolution, relatively low SNR and small RV separation, the maximum is obtained at a clear peak around the correct frequency. It seems the new periodogram performs reasonably well in this quite challenging case as well.

3.3. Periodic temperature variability

In addition to the examples above, we wished to test whether USuRPER is indeed sensitive also to other types of spectroscopic periodicities, not merely those related to periodic Doppler shifts. The periodic expansion and contraction phases of pulsating stars cause periodic Doppler shifts, but are also accompanied by cooling and heating. We therefore decided to simulate such periodic temperature changes, using the PHOENIX library, without the Doppler shift, so that the spectral features that change periodically would not be easily describable in a simple manner like Doppler shifts.

We have simulated a saw-tooth effective-temperature variability, with T_{eff} varying between 5000 K and 6000 K, and a period of 7 days, by a simple linear interpolation over the PHOENIX temperature grid. This is a rough approximation to typical T_{eff} variability of classical Cepheids (e.g. Andrievsky et al. 2005). We have simulated 15 random epochs, again over an interval of 100 days, with an SNR of 30 (Fig. 6). Fig. 7 focuses on a narrow wavelength range of 4952 – 4967 Å around the Iron c-line and shows how the spectrum changes as a result of the variable effective temperature (without the added noise). The dashed yellow line represents the spectrum of the lowest temperature simulated (5043 K) and the red dotted line shows the highest temperature (5936 K). A spectrum of a temperature in the middle (5486 K) is also plotted, with a blue line. The range of simulated temperatures is shaded in gray. One can see the minute changes in the equivalent widths of the lines caused by the varying effective temperature, without any bulk Doppler shift. Note also that different lines behave quite differently, and might even exhibit different trends in equivalent width, as the temperature varies.

Fig. 8 shows the result of the USuRPER periodogram applied to this dataset. In spite of the less favourable conditions, where there are less samples than the previous examples, and the SNR is not optimal, the peak at the correct period is evident, confirming that our novel periodogram performs well also in cases in which the periodicity is very different from simple Doppler shifts.

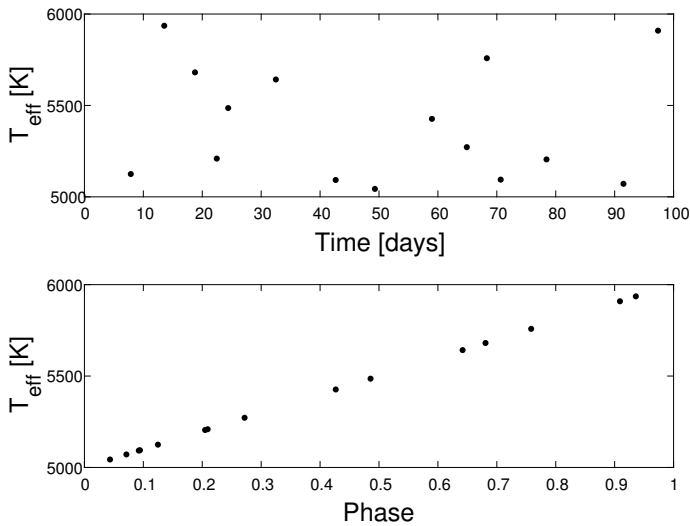


Fig. 6. Upper: the effective-temperature time series used in the periodic temperature variability simulation. Lower: the same effective-temperature time series phase-folded by the known 7-day period.

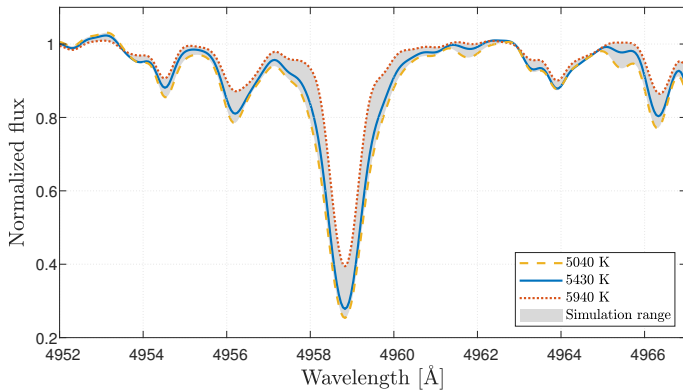


Fig. 7. A selected segment of the simulated spectra with periodic T_{eff} variability, before adding noise. The dashed yellow line corresponds to the spectrum with the lowest temperature (5043 K) and the dotted red line to the highest temperature (5936 K). The solid blue line represents a temperature in the middle (5486 K). The shaded area represents the range between the spectra with the extreme temperatures.

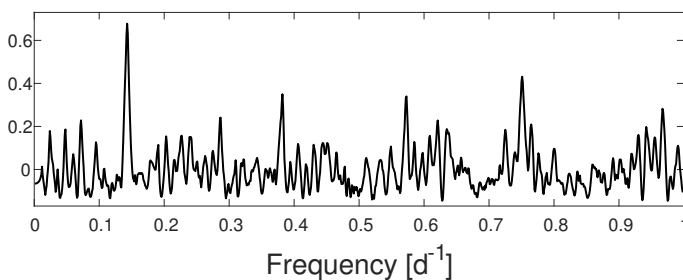


Fig. 8. USuRPER periodogram plot for the simulated temperature periodicity case. Note that the distance correlation values of USuRPER are normalized and therefore unitless.

3.4. Composite periodicity

After we have demonstrated that USuRPER is sensitive to both RV and temperature periodic variability, it is interesting to test how it performs when presented with a composite type of periodicity – periodic RV variability combined with periodic temperature variability, with different periods. To that end we have simulated again a set of 50 spectra. The simulated temperature

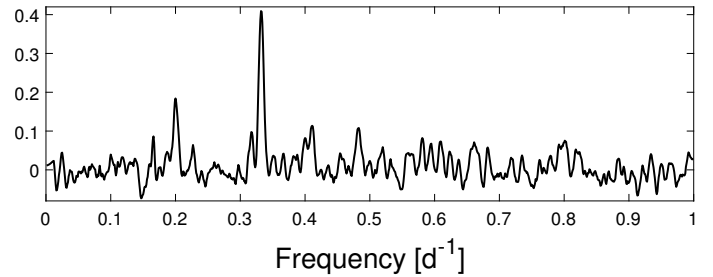


Fig. 9. USuRPER periodogram plot for the simulated composite temperature and RV periodicity case. Note that the distance correlation values of USuRPER are normalized and therefore unitless.

variability resembled the one in 3.3, but with a period of 5 days, whereas the RV variability was a sinusoidal variability similar to that in 3.1, with a period of 3 days. White Gaussian noise was added at a level corresponding to SNR of 100.

The two corresponding peaks, at frequencies $1/3$ and $1/5 \text{ d}^{-1}$, are clearly seen in the USuRPER periodogram of those data, in Fig. 9. They are not of the same prominence, though, probably reflecting the fact that the effect of temperature and RV periodicities, at the simulated amplitudes do not have the same impact on the overall variability of the spectrum. Nevertheless, the presence of both peaks in the periodogram shows that they did not somehow interfere in a destructive fashion that would make them disappear. This serves to show that USuRPER can also be used for cases of multiple periodicities. The case of a temperature periodicity combined with a RV periodicity of a different period can be encountered, e.g. in cases of Cepheids in spectroscopic binary stars (Szabados et al. 2013).

3.5. HD 115226

In the previous examples we have applied USuRPER on sequences of simulated spectra, which were obviously much more well-behaved than real-life data. We therefore looked for a publicly available real-life time-resolved spectroscopy dataset exhibiting spectral variability, preferably of a different type from those of the previous examples. We have finally decided to test USuRPER on observed spectra of a known rapidly oscillating Ap (roAp) star.

Broadly speaking, roAp stars are stars that exhibit very short-period photometric or RV variations, with periods of the order of minutes (e.g. Kurtz 1990). Ryabchikova et al. (2007) have further characterised the spectral variability of roAp stars by showing that absorption lines of some of the heavier chemical species (namely rare-element ions) perform periodic Doppler shifts, usually all with the same period but not with the same amplitude nor phase. This means that the overall spectrum shape changes periodically with a rather complicated pattern, which renders analysis by cross-correlation ineffective. Instead, the common approach is to analyse each individual line separately, measure its Doppler shift and analyse its periodicity.

Kochukhov et al. (2008) have observed the roAp star HD 115226 using HARPS (Mayor et al. 2003). They have obtained time-series spectroscopy of HD 115226 including 102 spectra, during a time interval of 4.3 hours, and performed a meticulous RV analysis of various absorption lines. The analysis yielded an estimated oscillation period of $10.87 \pm 0.01 \text{ min}$.

We have downloaded the 102 HARPS spectra, and applied USuRPER on this dataset. Based on table 3 of Kochukhov et al. (2008), we had restricted the wavelength range we analysed to

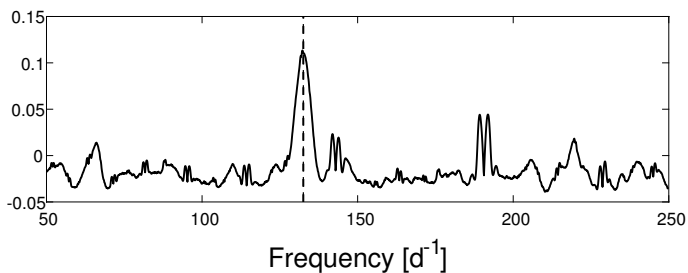


Fig. 10. USuRPER periodogram plot for the HARPS spectra of HD 115226. The dashed line represents the known period of 10.87 min (Kochukhov et al. 2008). Note that the distance correlation values of USuRPER are normalized and therefore unitless.

4900–5150 Å, where a few important Nd III lines are located. A wider wavelength range would have diluted the periodicity information, since most of the spectral features in other wavelengths do not exhibit periodicity. Knowing that we look for a phenomenon with a typical period of a few minutes, we ran USuRPER on a frequency range of 50–250 d⁻¹, corresponding to a period range of 5.76–28.8 min. Fig. 10 shows the resulting periodogram. The obvious maximum is at a frequency of 132.3 d⁻¹, corresponding to a period of 10.88 min, in agreement with the period Kochukhov et al. had obtained by their individual-line analysis.

4. Conclusion

The examples we have shown above attest to the wide potential of the USuRPER periodogram. We have shown that it performs well in cases of RV periodicities, composite SB2 spectra, and even complicated spectrum-shape patterns like periodic temperature changes. We have also demonstrated its performance in real-life cases of exotic variability like roAp stars. We provide our Python implementation of USuRPER in the form of a public GitHub repository².

In order to estimate the significance of peaks in the USuRPER periodogram, simple bootstrap-like permutation tests can be performed in which the time stamps of the individual spectra would be repeatedly randomly shuffled, in order to obtain the null distribution of the distance correlation values under the assumption of no dependence.

Since USuRPER does not provide any further information about the nature of the periodicity, except for the period and its significance, it is essentially useful as an exploratory tool. Once a prominent peak appears in the periodogram, further analysis is required in order to tell whether the observed object is a binary star (or exoplanet), a pulsating star, or maybe some other type of periodicity we have never encountered before.

An important application of USuRPER can be, for example, to use it in the analysis of the RVS, BP and RP spectra of *Gaia* (Gaia Collaboration 2016), or other large spectroscopic surveys with potentially multiple visits per object, e.g. APOGEE (Majewski et al. 2017) or LAMOST (Cui et al. 2012). Another interesting application might be the study of periodic stellar variability patterns, that might interfere with the detection of exoplanets through minute Keplerian RV variations (Boisse et al. 2011).

The USuRPER periodogram offers a completely new approach to study astronomical spectra. An approach that may very

well pave the way to new discoveries and insights, potentially ones that cannot be discovered in any other way.

Acknowledgements. We are grateful to Aviad Panahi for patiently examining our USuRPER code implementation, and to Dolev Bashi for reviewing and commenting on an early version of the manuscript. This research was supported by the ISRAEL SCIENCE FOUNDATION (grant No. 848/16). We also acknowledge partial support by the Ministry of Science, Technology and Space, Israel. The research is partly based on observations collected at the European Southern Observatory, La Silla, Chile (ESO program 079.D-0118). The analyses done for this paper made use of the code packages: Astropy (Astropy Collaboration 2013, 2018), NumPy (van der Walt et al. 2011), SciPy (Virtanen et al. 2020), and PyAstronomy (Czesla et al. 2019).

References

- Aerts, C., De Pauw, M., & Waelkens, C. 1992, A&A, 266, 294
- Andrievsky, S. M., Luck, R. E., & Kovtyukh V. V. 2005, AJ, 130, 1880
- Astropy Collaboration (Robitaille, T. P., et al.) 2013, A&A, 558, A33
- Astropy Collaboration (Price-Whelan, A. M., et al.) 2018, AJ, 156, 123
- Boisse, I., Bouchy, F., Hébrard G., et al. A&A, 528, A4
- Chaudhuri, A., & Hu, W. 2019, Compu. Stat. Data Anal., 135, 15
- Cui, X.-Q., Zhao, Y.-H., Chu, Y.-Q., et al. 2012, Res. Astron. Astrophys., 12, 1197
- Czesla, S., Schröter, S., Schneider, C. P., et al. 2019, Astrophysics Source Code Library [record ascl:1906.010]
- Ferraz-Mello, S. 1981, AJ, 86, 619
- Gaia Collaboration (Brown, A. G. A., et al.) 2016, A&A, 595, A1
- Huo, X., & Székely, G. J. 2016, Technometrics, 58, 435
- Husser, T.-O., Wende-von Berg, S., Dreizler, S., et al. 2013, A&A, 553, A6
- Kochukhov, O., Ryabchikova, T., Bagnulo, S., Lo Curto, G. 2008, A&A, 479, L29
- Kurtz, D. W. 1990, ARA&A, 28, 607
- Lyons, R. 2013, Ann. Probab., 41, 3284
- Majewski S. R., Schiavon, R. P., Frinchaboy, P. M., et al. 2017, AJ, 154, 94
- Mayor, M., Pepe, F., Queloz, D., et al. 2003, The Messenger, 114, 207
- Ryabchikova, T., Sachkov, M., Kochukov, M., & Lyashko D. 2007, A&A, 473, 907
- Szabados, L., Derekas, A., Kiss, L. L., et al. 2013, MNRAS, 430, 2018
- Székely, G. J., & Rizzo, M. L. 2013, J. Multivar. Anal., 117, 193
- Székely, G. J., & Rizzo, M. L. 2014, Ann. Stat., 42, 2382
- Székely, G. J., Rizzo, M. L., & Bakirov, N. K. 2007, Ann. Stat., 35, 2769
- Tonry J., & Davis M. 1979, AJ, 84, 1511
- van der Walt, S., Colbert, S. C., & Varoquaux G. 2011, Comput. Sci. Eng., 13, 22
- Virtanen P., Gommers, R., Oliphant, T. E., et al. 2020, Nat. Methods, 17, 261
- Zechmeister, M., & Kürster, M. 2009, A&A, 496, 577
- Zinger, A. A., Kakosyan, A. V., & Klebanov, L. B. 1992, J. Soviet Math., 59, 914
- Zucker, S. 2018 MNRAS, 474, L86
- Zucker, S. 2019 MNRAS, 484, L14
- Zucker S., & Mazeh T. 1994, ApJ, 420, 806

² USuRPER is available as part of the SPARTA package, at <https://github.com/SPARTA-dev/SPARTA>.